



## Synthesis and Photoluminescent Properties of Sm<sup>3+</sup> - Doped SnO<sub>2</sub> Nanoparticles

*B. M. Morais Faustino, P. J. S. Foot,\* , R.A. Kresinski  
Materials Research Center, SEC Faculty, Kingston University London  
Penrhyn Road, Kingston upon Thames, Surrey KT1 2EE  
United Kingdom*

*\* Author for correspondence. Email: [P.J.Foot@kingston.ac.uk](mailto:P.J.Foot@kingston.ac.uk)*

### **Abstract**

SnO<sub>2</sub> ceramic nanoparticles homogeneously doped with Sm<sup>3+</sup> ions were synthesized *via* a sol-gel method, followed by drying and annealing in air. X-ray diffractometry, FT-IR spectrometry and transmission electron microscopy were used to characterize the nanoparticulate samples. After annealing, both doped and undoped SnO<sub>2</sub> nanopowders were shown to adopt the rutile tetragonal crystal form and to exhibit characteristic Sn-O-Sn vibrations. The average particle size was found to be in the region of 23–28 nm. Photoluminescence analysis at room temperature demonstrated strong enhancement of the visible emission from Sm<sup>3+</sup>, *via* energy transfer from the SnO<sub>2</sub> host matrix to the dopant. The maximum emission efficiency was observed for a concentration of 1.5 atom % Sm<sup>3+</sup>.

## 1. Introduction

Lanthanides ( $\text{Ln}^{3+}$ ) are well-known for their applications in optoelectronics, owing to their remarkable luminescence properties [1]. Their stabilities, emission lifetimes and quantum yields are advantageous for many potential applications in optoelectronic devices [2] and optical communications [3]. However a drawback of lanthanides is their weak absorption for direct excitation due to the spin-forbidden nature of  $f-f$  transitions, which limits their efficiency [1-5].

The demand for an improvement in energy efficiency in optoelectronic devices has prompted extensive research into enhancement of luminescence by host sensitization *via* energy transfer mechanisms [1,4,5]. Successful energy transfer from the triplet states of organic ligands to their neighboring ions has been widely reported for metal-organic complexes, but these materials often lack thermal stability, which is vital for many solid-state device applications [6,7].

The incorporation of  $\text{Ln}^{3+}$  ions into nano-scale metal oxide ceramic powders has the potential to enhance their luminescence *via* host-sensitization. Nano-scale oxide semiconductors perform differently from their bulk counterparts because of quantum size effects [8]. The ease of tailoring their luminescence *via* structural and morphological control, their electro- and photo-excitability and their long-term stability make them good hosts for sensitized emission [8-10].  $\text{SnO}_2$  is a well-known n-type semiconductor with a wide band gap ( $E_g=3.6\text{eV}$  at 300K). Its mechanical, optical, thermal and chemical properties could render it an excellent host sensitizer for  $\text{Ln}^{3+}$ . Literature reports on the optical properties of  $\text{SnO}_2$  ceramic nanoparticles are relatively scarce. Studies of  $\text{SnO}_2$  doped with ions such as Er[11], Dy[12], Eu[13], Sb[14] and Mg[15] have been reported, but to the best of our knowledge, very few reports exist of host sensitization energy

transfer studies involving SnO<sub>2</sub> nanocrystals and Sm<sup>3+</sup> ions [16]. Sensitized emission from semiconductors has mainly been reported for TiO<sub>2</sub> host structures[5], but in most cases the semiconductor was embedded in a partially-crystalline or amorphous matrix, and the resulting reduction in site homogeneity and symmetry led to broadening of the emission peaks at room temperature.

The preparation of ceramic nanoparticles *via* the sol-gel route usually has a low cost, as it involves the use of inexpensive precursors and solvents and requires only mild reaction conditions using common laboratory apparatus. In this work, we report a facile sol-gel synthesis of pure and samarium-doped SnO<sub>2</sub> nanoparticles. Photoluminescence (PL) enhancement of Sm<sup>3+</sup> ions *via* energy transfer from the SnO<sub>2</sub> semiconductor host was observed, with sharp, well-resolved emission lines at room temperature. The photoluminescence intensity was dependent on the amount of energy transferred from the host to the dopant and the emission enhancement and quenching were tunable by adjusting the Sm<sup>3+</sup> content. In addition to the PL studies, we also report the morphological and structural effects of doping, and propose a simple mechanism of energy-transfer *via* host sensitization.

## **2. Experimental**

### **2.1 Preparation of Sm<sup>3+</sup> - doped SnO<sub>2</sub> nanocrystals.**

All chemicals were purchased from Sigma-Aldrich UK, and used as-received with no further purification. Sm(III)-doped SnO<sub>2</sub> nanoceramic particles were prepared as follows: 0.2 mol of tin (IV) chloride pentahydrate was dissolved in 100mL of methanol under vigorous stirring for 15 min to form a transparent solution. Samarium (III) chloride hexahydrate was added to the above solution

to achieve doping concentrations between 0-3.0 at.% Sm with respect to the tin content. After a further 15 min stirring, 2 mol dm<sup>-3</sup> aqueous ammonia was added dropwise until pH 8 was reached. The addition rate of aqueous ammonia was adjusted to 0.5 mL min<sup>-1</sup> in order to maintain the chemical homogeneity of the forming gel. The intermediate hydroxide product was then stirred for 1 h at 353K before the solvent was allowed to evaporate overnight. The resulting xerogel was washed several times with methanol and distilled water to remove any unreacted metal halides. After drying at 393K for 1h, the gel powder was ground in a mortar and finally annealed at 673K for 3h to yield a very pale-yellow nanocrystalline tin oxide product.

## 2.2 Characterization

X-Ray powder diffraction measurements were performed on all samples with a Bruker AXS D8 Advance powder X-ray diffractometer using Cu K<sub>α</sub> radiation ( $\lambda=0.1542 \text{ \AA}$ ) from a source run at 40kV and 25mA, in the diffraction angle range 15 to 70° 2-theta. The average crystallite size was estimated using the Scherrer equation:

$$L=K\lambda/\beta\cos\theta$$

where  $L$  is the crystallite size,  $K$  is a geometric factor (taken here as 0.9),  $\lambda$  is the x-ray wavelength,  $\beta$  is the peak broadening in radians at half the maximum height and  $\theta$  is the diffraction angle. The specific surface areas of the nanocrystallites were measured by the BET technique using a Belsorp Mini II instrument from BEL, Japan. Attenuated total reflectance infrared spectroscopy was performed on all samples using a diamond crystal Thermo Scientific Nicolet iS5 iD5 ATR spectrophotometer. The spectra were recorded in transmission mode with a resolution of 4cm<sup>-1</sup> between 500 and 4000cm<sup>-1</sup>. The morphology of the particles was observed by transmission electron microscopy using a JEOL

JEM1010 with an accelerating voltage of 80kV. The powder was dispersed by serial dilutions in methanol and then prepared for TEM by placing a drop of each dilution onto a Formvar® support film copper grid (Agar Scientific Ltd.). No further treatment or staining was required. Photoluminescence studies of solid solution-cast films on quartz slides were carried out at room temperature, using a Varian Cary Eclipse fluorescence spectrophotometer with a 300W Xe lamp excitation source. The spectrometer was calibrated using the fluorescent emission of Rhodamine-B and appropriate correction curves. Measurements were performed with a slit setting of 1.5nm for excitation and emission at a scan rate of 120nm min<sup>-1</sup>.

### **3. Results and Discussion**

#### **3.1 Characterization of Sm<sup>3+</sup> - doped SnO<sub>2</sub> nanocrystals**

##### **3.1.1. Morphology, crystal properties and UV-visible absorption analysis.**

The XRD patterns of doped and undoped SnO<sub>2</sub> nanoparticles are shown in Fig. 1. The peaks were assigned to the (110), (101), (200), (211), (220), (002) and (310) diffraction planes of tetragonal rutile-structured SnO<sub>2</sub> [JCPDS PDF 41-1445] [17]. No traces of additional peaks characteristic of impurities such as samarium oxide or stoichiometric samarium tin oxides were observed, indicating that the dopant was distributed throughout the SnO<sub>2</sub> phase. For all samples, doped and undoped, the broadening of the diffraction peaks indicated nanoscale crystal dimensions. The average crystallite size calculated by means of the Scherrer equation was in the region of 23 to 28 nm, as indicated in Table 1. The data suggest that doping Sm<sup>3+</sup> into SnO<sub>2</sub> increased the average particle size, although it is not yet known whether this was due to a reduction in the nucleation rate or an increase in the growth rate of the nanoparticles. The fractional doping of samarium per tin atom was confirmed by inductively-

coupled plasma (ICP-AES) analysis after dissolution of the samples in aqueous HCl.

The band gap values shown in Table 1 were obtained using UV-visible absorption spectroscopy, by extrapolating the steep absorption edges to meet the sample baseline, and conversion of the corresponding absorption onset wavelength to energy using Planck's equation. There was a significant blue-shift of the band gap transitions for doped nanocrystalline SnO<sub>2</sub> relative to that of bulk SnO<sub>2</sub> (3.6 eV), which is consistent with a quantum confinement effect. The band gaps of the Sm-SnO<sub>2</sub> nanoparticles varied from 3.71 eV for 0.5 atom % Sm to 3.84 eV for 3 atom % Sm; their monotonic increase with the dopant concentration tends to support our belief that the Sm<sup>3+</sup> ions homogeneously entered the crystal lattice of SnO<sub>2</sub> rather than forming a separate phase.

A typical TEM micrograph of SnO<sub>2</sub> #2 is shown in Fig. 2, with a Gaussian profile (inset) showing a fairly narrow distribution of particle sizes. The TEM images revealed nearly-spherical particles with sizes in the range of 23-28 nm. Some degree of agglomeration became noticeable with increasing Sm<sup>3+</sup> content.

Fig. 3 shows a typical ATR-IR spectrum of the Sm<sup>3+</sup> doped SnO<sub>2</sub> nanoparticles, illustrating the effect of annealing on the chemical composition of the sample.

The broad band peaking around 3100 and 3300 cm<sup>-1</sup> is attributable to a ν<sub>OH</sub> stretching vibration. Some residual bands of ν<sub>CH<sub>3</sub></sub> are also seen at 3000 cm<sup>-1</sup>.

Other bands corresponding to overtones of ν<sub>OH</sub> and δ<sub>OH</sub> are detected at 1400, 1131 and 1012 cm<sup>-1</sup>. The strong band at 653 cm<sup>-1</sup> is associated with asymmetric Sn-O-Sn stretching [18]. A comparison between spectra (a) before and (b) after annealing confirms the elimination of organic residues and the successful condensation of the hydroxyl groups to form Sn-O-Sn bridges.

Annealing is therefore essential during sample preparation in order to ensure the purity of the tin oxide ceramic particles.

### 3.1.2. Photoluminescence sensitization of Sm<sup>3+</sup> - doped SnO<sub>2</sub> nanocrystals

The emission spectra of our materials featured three peaks at 545, 595 and 695 nm, attributed to electronic transitions from the excited <sup>4</sup>G<sub>5/2</sub> state to the <sup>6</sup>H<sub>5/2</sub>, <sup>6</sup>H<sub>7/2</sub>, and <sup>6</sup>H<sub>9/2</sub> states, respectively. Fig. 4 shows the excitation spectrum of a typical sample with a broad peak centered at 300 nm, as well as the sensitized emission spectrum of Sm<sup>3+</sup>. Since the crystallinity would be expected to affect the PL efficiency, all samples undergoing PL analysis were annealed at a standard temperature of 673K.

Efficient sensitized emission from the Sm<sup>3+</sup> dopant in the nanocrystals was achieved upon excitation above the band gap energy of the SnO<sub>2</sub> host. When excited in this way, the Sm<sup>3+</sup> visible emission in the yellow-orange region of the spectrum was enhanced, relative to the much weaker emission obtainable *via* direct excitation of the Sm<sup>3+</sup> ions at a wavelength of 402nm. Fig. 5 provides a comparison of the emission intensity between the two pathways of excitation and illustrates energy transfer from host to dopant, with an efficiency exceeding that of direct excitation *via* the parity-forbidden f-f transitions of Sm<sup>3+</sup>. In fact, excitation lines arising from f-f transitions were barely detectable because of the much more efficient host-to-dopant pathway of excitation.

To investigate the effect of the proportion of Sm<sup>3+</sup> dopant on the PL intensity, samples were doped at different concentrations (Table 1). For the <sup>4</sup>G<sub>5/2</sub> -> <sup>6</sup>H<sub>7/2</sub> transition, maximum emission intensity was found to occur at around 1.5 atom % Sm<sup>3+</sup>, as shown in Fig. 6. This can be explained by assuming energy transfer as described by Dexter [19], in which the mechanism is a short-range nonradiative exchange interaction. Therefore, both the Sn-Sm ionic distance and the distance between Sm<sup>3+</sup> centers might be critical; the latter because it may

contribute to quenching by cross-relaxation of neighboring samarium ions when they are present in *excess*. This seems to be manifest at doping concentrations above 1.5 atom %, beyond which a diminution of photoluminescence efficiency is noticeable. The calculated critical distance between  $\text{Sm}^{3+}$  ions at 1.5% is about 9.2 Å (0.92 nm); such a range would be consistent with Dexter's model for energy transfer. This is a little surprising, since longer-range mechanisms involving electric multipole transitions might be expected to play a role in quenching the excited lanthanide ions.

Some other photoluminescence enhancement studies of  $\text{Sm}^{3+}$  in oxide hosts have been reported [8, 20-22]; however these were postulated to proceed *via* energy transfer mechanisms involving complex networks. In most of these cases, emission line broadening and unidentified shoulders are often observed, and are ascribed to structural lattice defects, oxygen vacancies and surface states. Luo *et al* [20] reported fewer defects and less obvious shoulders at 10K for  $\text{Sm}^{3+}$ -doped  $\text{TiO}_2$ , but weaker host-sensitized luminescence was detected. Titania nanocrystals often undergo structural phase changes during the annealing process [23], and control of structural defects and surface states is difficult. Several cases have been reported of lanthanide doping of  $\text{TiO}_2$  nanocrystals to favor one phase over the other in respect to desirable optical properties [5, 20, 22].  $\text{SnO}_2$  nanocrystals, on the other hand, show a single rutile structure. However,  $\text{Sn}^{4+}$  and  $\text{Sm}^{3+}$  ions have different covalent and ionic radii (0.71Å and 0.96Å, respectively) and for every Sn substitution by Sm generates oxygen vacancies to keep overall neutrality, creating local lattice distortion. Consequently, oxygen vacancies cannot be excluded when accounting for the slight broadening of the  $\text{Sm}^{3+}$  emission peaks, and they may indeed mediate the energy transfer from host to dopant, as claimed by Singh *et al*. [16] for  $\text{SnO}_2$  and by Liu *et al*. [5] for ZnO and  $\text{TiO}_2$ . Singh and his co-workers [16] recently

reported sensitized luminescence of Sm dopant in SnO<sub>2</sub> nanoparticles; their sensitized emission spectra were broad and not well resolved, but those authors discovered important annealing consequences including the removal of quenching surface hydroxides, in contrast to earlier research [24]. Furthermore, given the clear enhancement in photoluminescent efficiency in the spectra reported here, along with the observed crystal-field splittings not previously detected via direct excitation, a possible interpretation of the splitting and sharp emission is the highly crystalline surrounding environment of the Sm<sup>3+</sup> lattice sites within the ceramic nanocrystals [25].

### 3.2 Sensitized energy-transfer mechanism

Fig. 7 illustrates the energy transfer from host SnO<sub>2</sub> to Sm<sup>3+</sup> ions, wherein excitation above the band gap energy of SnO<sub>2</sub> leads to electrons in the valence band being promoted to the conduction band, generating holes in the valence band. The energy resulting from the recombination of electrons and holes in the host is required to match that of the excited state of Sm<sup>3+</sup> ions so as to allow energy transfer from host to lanthanide in a nonradiative way. We believe this nonradiative energy transfer occurs at short-range (<10Å or 1nm) between Sm<sup>3+</sup> and Sn<sup>4+</sup> ions, in accordance with Dexter's model [19]. Given the evident effect of samarium doping concentration on the intensity of PL emission, we believe a double energy transfer may occur between Sn<sup>4+</sup> and Sm<sup>3+</sup> and, as this very short-range process requires the overlap of wavefunctions between the two species, the rate of energy transfer by electronic exchange is, on Dexter's model, an exponential function of their separation.

The energy corresponding to excitation of our nanocrystals at 300nm exceeds the band gap energy of the SnO<sub>2</sub> nanocrystals, which in turn, is higher than that of bulk SnO<sub>2</sub>; this is consistent with the notion of the energy being transferred to

the excited state of a neighboring  $\text{Sm}^{3+}$  ion. Excitation at 300nm (4.1eV) might possibly result in nonradiative transfer to  $^4\text{D}_{7/2}$ , the next available excited state of  $\text{Sm}^{3+}$ . We propose that non-radiative decay of energy from  $^4\text{D}_{7/2}$  to  $^4\text{G}_{5/2}$  precedes the production of orange-yellow emission from the lowest excited state of  $\text{Sm}^{3+}$  to the lowest available ground state, giving rise to emission lines corresponding to the transitions:  $^4\text{G}_{5/2} \rightarrow ^6\text{H}_j$ ,  $J= 5/2, 7/2, 9/2$  and  $11/2$ .

#### **4. Conclusion**

The synthesis of  $\text{Sm}^{3+}$ -doped  $\text{SnO}_2$  *via* a sol-gel method has produced uniform spherical nanoparticles with a narrow size distribution. XRD all showed the same rutile crystalline patterns for doped samples at different concentrations, very similar to that of undoped  $\text{SnO}_2$ . The average particle size was determined by XRD and TEM, with average values in the region of 23-28nm. Dopant concentration was found to have a prominent role in determining crystallite size. The band structure of the particles showed a strong quantum confinement effect, and the excited electronic states were high enough to allow energy transfer from the host to  $\text{Sm}^{3+}$ . The observed increase in the relative intensity of photoluminescence data revealed strong enhancement due to host sensitization, with a maximum intensity at around 1.5 atom %  $\text{Sm}^{3+}$ ; higher Sm contents resulted in quenching effects and possible increases in oxygen vacancies and surface defects.

#### **Acknowledgement**

We thank Kingston University for the award of a Research Scholarship to support BMF.

## References

- [1] A. J. Kenyon, Recent developments in rare-earth doped materials for optoelectronics. *Progress in Quantum Electronics*, 26 (2002) 225-84.
- [2] L. Armelao, S. Quici, F. Barigelletti, G. Accorsi, G. Bottaro, M. Cavazzini, E. Tondello, Design of luminescent lanthanide complexes: From molecules to highly efficient photo-emitting materials. *Coord. Chem. Rev.* 254 (2010) 487-505.
- [3] J. G. Bünzli, S. V. Eliseeva, Lanthanide NIR luminescence for telecommunications, bioanalyses and solar energy conversion. *Journal of Rare Earths* 28 (2010) 824-42.
- [4] J. G. Bünzli, S. Comby, A. Chauvin, C. D. B. Vandevyver, New opportunities for lanthanide luminescence, *Journal of Rare Earths*. 25 (2007) 257-74.
- [5] Y. Liu, W. Luo, H. Zhu, X. Chen, Optical spectroscopy of lanthanides doped in wide band-gap semiconductor nanocrystals. *J. Lumin.* 131 (2011) 415-22.
- [6] L. Fu, X. Wen, X. Ai, Y. Sun, Y. Wu, J. Zhang, Y. Wang, Efficient two-photon-sensitized luminescence of a europium(III) complex. *Angewandte Chemie International Edition* 44 (2005) 747-50.
- [7] V. Vicinelli, P. Ceroni, M. Maestri, V. Balzani, M. Gorka, F. Vögtle, Luminescent lanthanide ions hosted in a fluorescent polylysine dendrimer: Antenna-like sensitization of visible and near-infrared emission. *J. Am. Chem. Soc.* 124 (2002) 6461-8.
- [8] Y. Liu, F. Yang, X. Yang, Size-controlled synthesis and characterization of quantum-size SnO<sub>2</sub> nanocrystallites by a solvothermal route. *Colloid. Surf. A-Physicochem Eng. Asp.* 312 (2008) 219-25.
- [9] A. P. Alivisatos, Semiconductor clusters, nanocrystals, and quantum dots. *Science* 271 (1996) 933-937.
- [10] Lin Tao, Wang Neng, Han Min, Xu Jun, Chen Kun-Ji, Synthesis, structures and luminescence properties of SnO<sub>2</sub> nanoparticles. *Acta Phys. Sinica* 58 (2009) 5821-5.
- [11] S. Sambasivam, S. B. Kim, J. H. Jeong, B. C. Choi, K. T. Lim, S. S. Kim, T. K. Song, S. Effect of Er<sup>3+</sup> doping in SnO<sub>2</sub> semiconductor nanoparticles synthesized by sol-gel technique. *Curr. Appl. Phys.* 10 (2010) 1383-6.
- [12] F. Gu, S. Fen Wang, M. K. Lü, Y. Xin Qi, G. Jun Zhou, D. Xu, D. Rong Yuan, Preparation and luminescence characteristics of nanocrystalline SnO<sub>2</sub> particles doped with Dy<sup>3+</sup>. *J. Cryst. Growth* 255 (2003) 357-60.
- [13] M. Chowdhury, S. K. Sharma, S.P. Lochab, Thermoluminescence glow curve analysis of gamma-irradiated Eu<sup>3+</sup> doped SnO<sub>2</sub> composites. *Ceram. Int.* 42 (2016) 5472-78.
- [14] X. Liu, J. Chen, W. Sang, B. Qin, Complexation-coprecipitation synthesis and characterization of erbium and antimony doped SnO<sub>2</sub> conductive nanoparticles. *J. Rare Earths* 25, Supplement 1 (2007) 72-6.

- [15] X. Li, R. Deng, B. Yao, Z. Ding, J. Qin, Q. Liang, Effect of Mg doping on optical and electrical properties of SnO<sub>2</sub> thin films: An experiment and first-principles study. *Ceram. Int.* 42 (2016) 5299-5303.
- [16] L. P. Singh, M. N. Luwang and S. K. Srivastava, Luminescence and photocatalytic studies of Sm<sup>3+</sup> ion doped SnO<sub>2</sub> nanoparticles. *New Journal of Chemistry*, 38 (2014) 115-121.
- [17] A. A. Bolzan, C. Fong, B. J. Kennedy, C. J. Howard, Structural studies of rutile-type metal dioxides. *Acta Crystallographica Section B* 53 (1997) 373-80.
- [18] D. Amalric-Popescu, F. Bozon-Verduraz, Infrared studies on SnO<sub>2</sub> and Pd/SnO<sub>2</sub>. *Catalysis Today* 70 (2001) 139-54.
- [19] D. L. Dexter, A Theory of Sensitized Luminescence in Solids. *J. Chem. Phys.* 21(1953) 836–850.
- [20] W. Q. Luo, R. F. Li, X. Y. Chen, Host-Sensitized Luminescence of Nd<sup>3+</sup> and Sm<sup>3+</sup> Ions Incorporated in Anatase Titania Nanocrystals. *J. Phys. Chem. C* 113 (2009) 8772-7.
- [21] A. C. Yanes, J. Mendez-Ramos, J. del-Castillo, J. J. Velazquez, V. D. Rodriguez, Size-dependent luminescence of Sm<sup>3+</sup> doped SnO<sub>2</sub> nano-particles dispersed in sol-gel silica glass. *Appl. Phys. B-Lasers Opt.* 101 (2010) 849-54.
- [22] L. Hu, H. Song, G. Pan, B. Yan, R. Qin, Q. Dai, L. Fan, S. Li, X. Bai, Photoluminescence properties of samarium-doped TiO<sub>2</sub> semiconductor nanocrystalline powders. *J. Lumin.* 127 (2007) 371-6.
- [23] U. Diebold, The surface science of titanium dioxide. *Surf. Sci. Rep.* 48 (2003) 53-229
- [24] F. Gu, S. F. Wang, C. F. Song, M. K. Lü, Y. X. Qi, G. J. Zhou, D. Xu, D. R. Yuan, Synthesis and luminescence properties of SnO<sub>2</sub> nanoparticles. *Chem. Phys. Lett.*, 372 (2003) 451-454.
- [25] X. Y. Chen and G. K. Liu, The standard and anomalous crystal-field spectra of Eu<sup>3+</sup>. *J. Sol. State Chem.*, 178 (2005) 419-428.

## Figure Captions

Fig. 1 – Powder X-ray diffractograms of SnO<sub>2</sub>:Sm<sub>x</sub> (x= 0%, 0.5%, 1.5%, 2.5% and 3%) nanoparticles.

Fig. 2 – TEM micrograph of sample #2 nanoparticles, with an inset size-distribution plot.

Fig. 3 – ATR-IR spectra of sample #2 (a) before and (b) after annealing at 673K

Fig. 4 – Excitation (left) and emission (right) spectra of SnO<sub>2</sub>:Sm nanoparticles (x= 1.5%) at room temperature.

Fig. 5 – PL emission spectra of SnO<sub>2</sub>:Sm<sup>3+</sup> *via* direct excitation at 402nm and *via* host-sensitization at 300 nm. The top curve shows the emission of the <sup>4</sup>G<sub>5/2</sub> → <sup>6</sup>H<sub>7/2</sub> transition with varying Sm content.

Fig. 6 – Stacked plot showing PL emission spectra of SnO<sub>2</sub>:Sm as a function of Sm<sup>3+</sup> concentration when excited above the band gap energy of SnO<sub>2</sub>.

Fig. 7 – Proposed mechanism of energy transfer (ET) between SnO<sub>2</sub> host-sensitizer and Sm<sup>3+</sup> ions. Curly arrows denote nonradiative transitions and straight arrows denote radiative transitions.

**Table 1. Dependence of crystallite size and band gap of SnO<sub>2</sub> nanoparticles on the atomic concentration of samarium dopant.**

<b>Sample</b>	<b>Sm<sup>3+</sup> (%)</b>	<b>Average Crystallite Size (nm)</b>	<b>Band gap (eV)</b>
#0	0	21	3.68
#1	0.5	23	3.71
#2	1	23	3.71
#3	1.5	24	3.74
#4	2	25	3.76
#5	2.5	26	3.80
#6	3	28	3.84

Figure 1

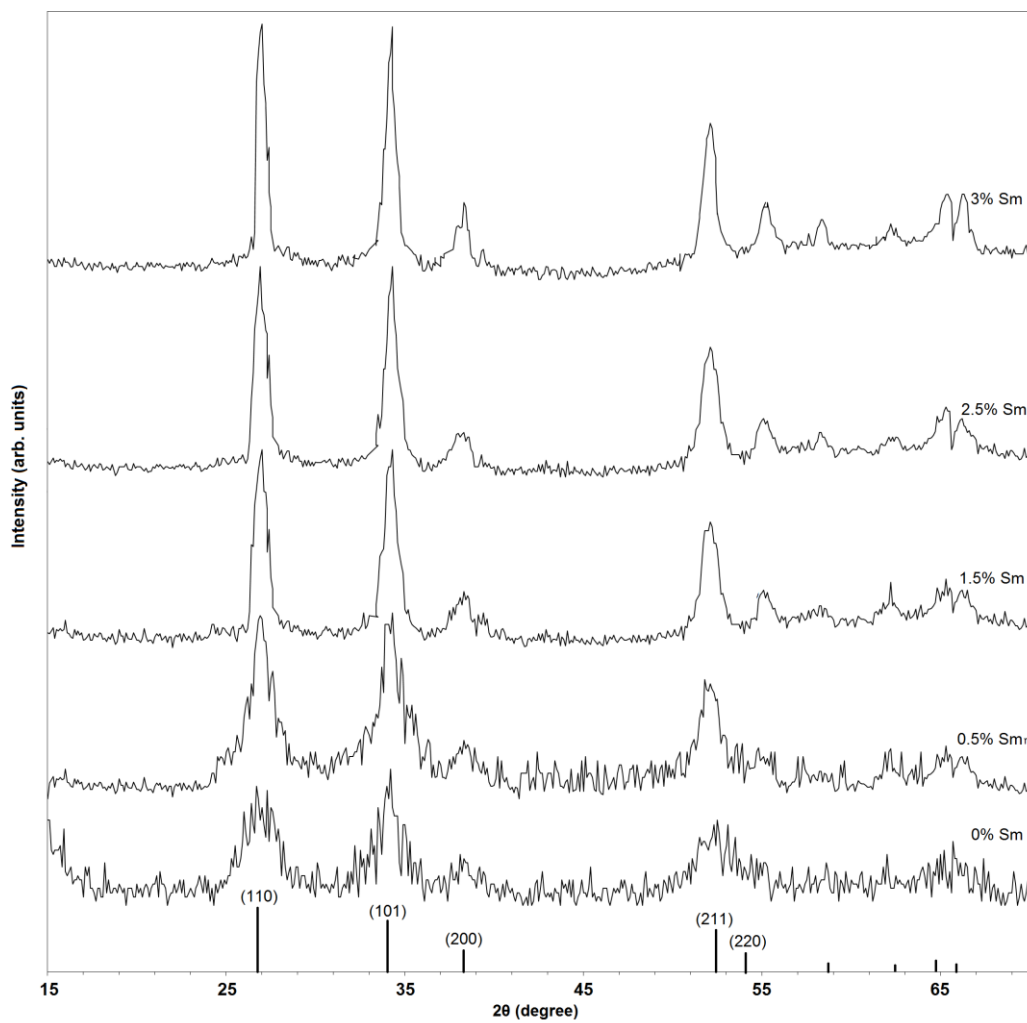


Figure 2

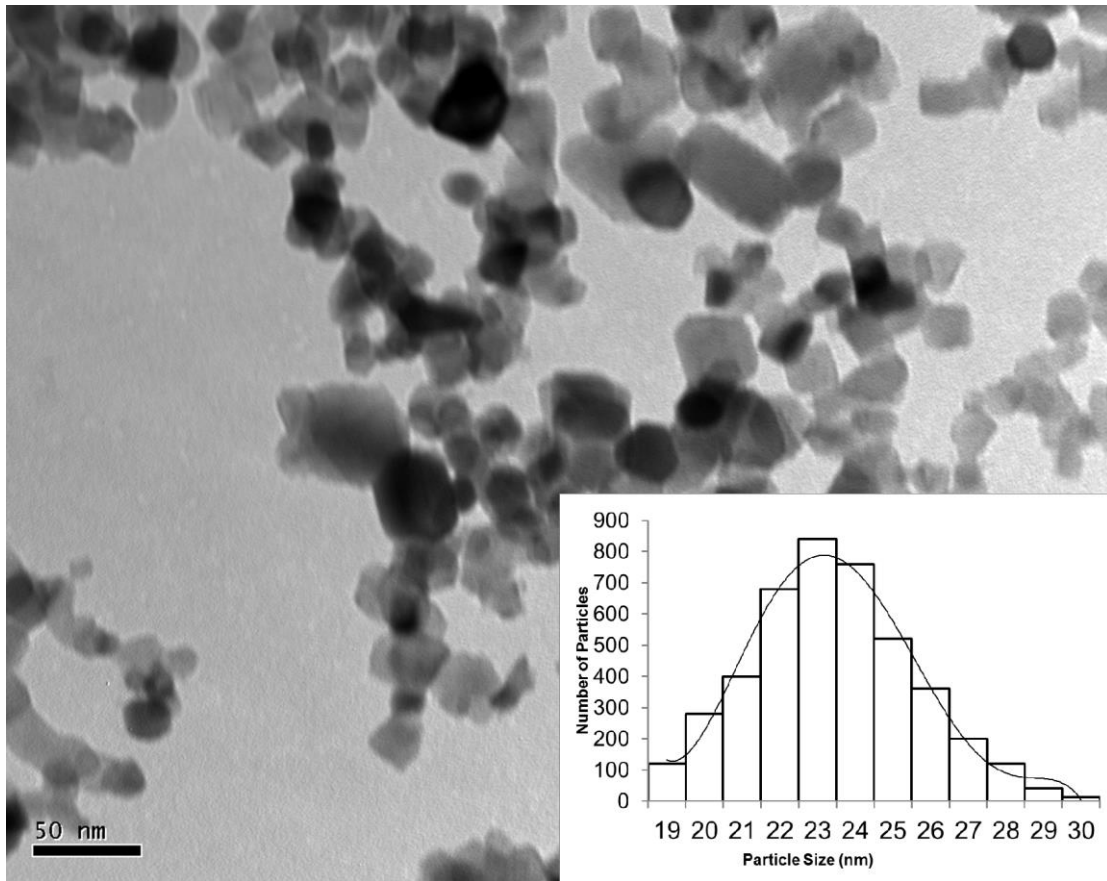


Figure 3

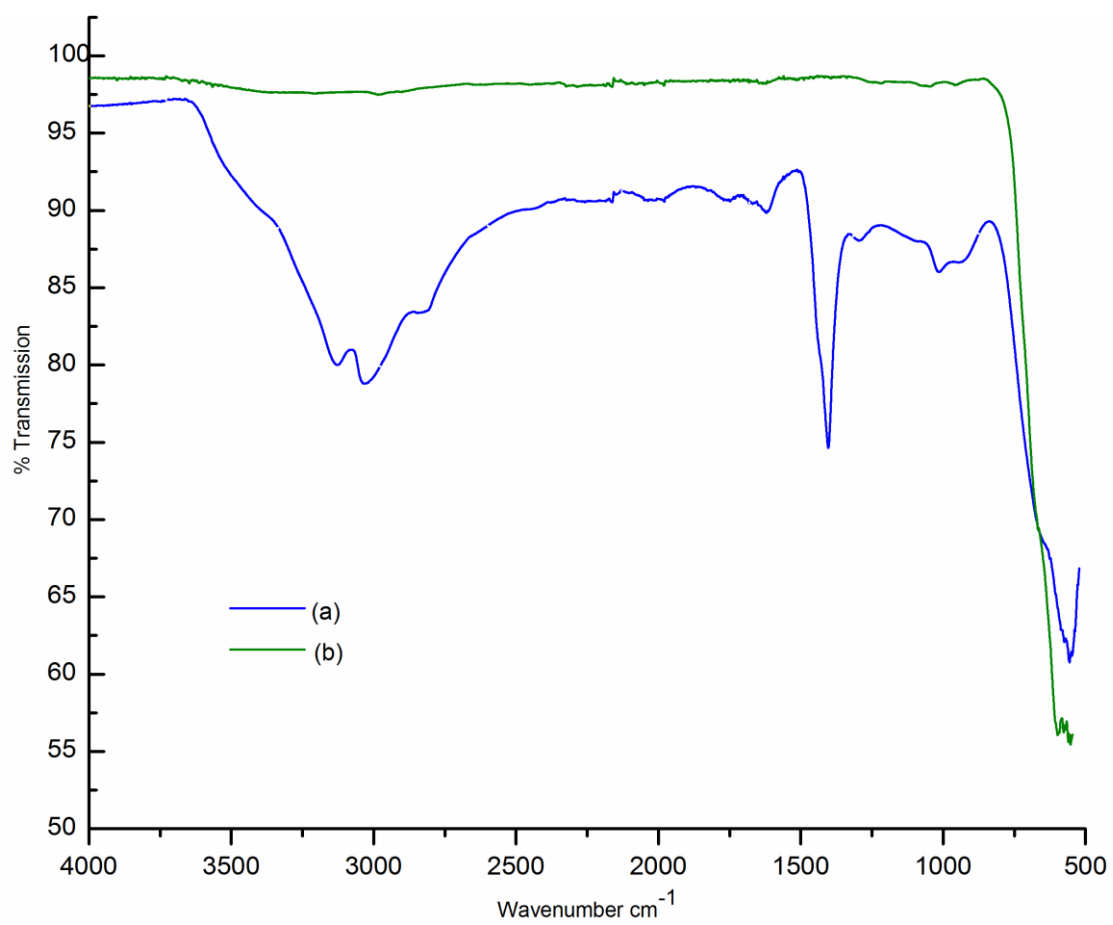


Figure 4

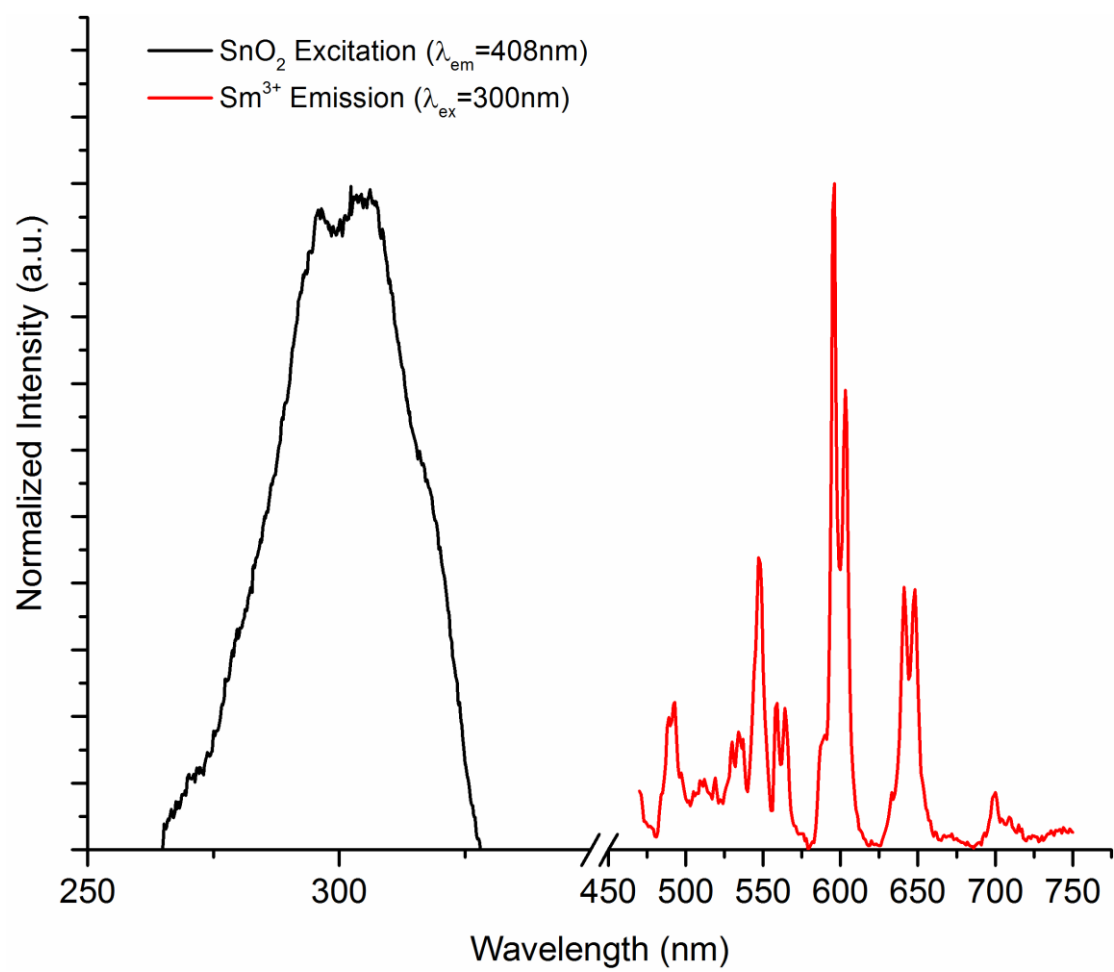


Figure 5

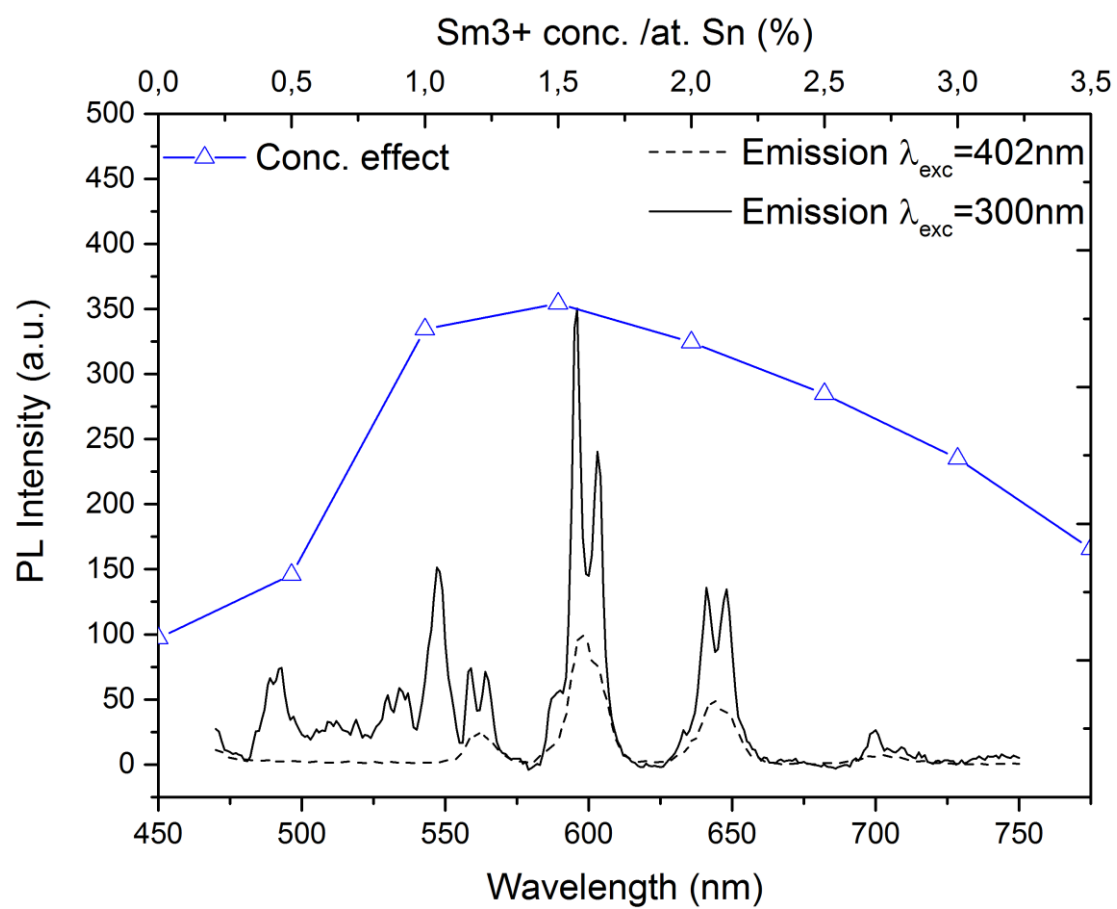


Figure 6

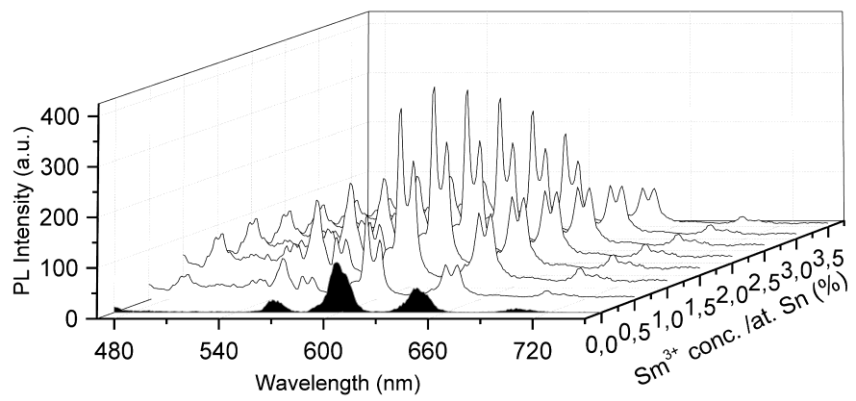


Figure 7

